Wenwu Zhang*

Y. Lawrence Yao

Department of Mechanical Engineering,
Columbia University, New York, NY 10027

I. C. Noyan

Thin Film Metallurgy Department, IBM T. J.
Watson Research Center
Yorktown Heights, NY 10598

Microscale Laser Shock Peening of Thin Films, Part 2: High Spatial Resolution Material Characterization

Microscale Laser Shock Peening (LSP) is a technique that can be potentially applied to manipulate the residual stress distributions in metal film structures and thus improve the reliability of micro-devices. This paper reports high-spatial-resolution characterization of shock treated copper thin films on single-crystal silicon substrates, where scanning x-ray microtopography is used to map the relative variation of the stress/strain field with micron spatial resolution, and instrumented nanoindentation is applied to measure the distribution of hardness and deduce the sign of the stress/strain field. The measurement results are also compared with 3-D simulation results. The general trends in simulations agree with those from experimental measurements. Simulations and experiments show that there is a near linear correlation between strain energy density at the film-substrate interface and the X-ray diffraction intensity contrast. [DOI: 10.1115/1.1645879]

1 Introduction

In recent years, failure and reliability problems in MEMS have been attracting increased attention [1,2]. While the dominant material in MEMS is silicon, metal and metallic thin film structures are often indispensable, and metal is a better choice for some applications. Some of the metal microstructures, such as micro-gears and micro-switches, experience cyclic loading in service. To increase the reliability of the system, wear resistance and fatigue performance of these metal structures should be improved.

Microscale Laser Shock Peening (LSP) can effectively induce favorable residual stress distributions in bulk metal targets with micron-level spatial resolution [3,4]. It may also potentially be used to improve the wear resistance and fatigue performance of the metal film structures. In Part I of this paper, microscale LSP of copper thin films on silicon substrates are described and global curvature measurements are used to prove that compressive residual stresses can be induced in the thin film which are balanced by tensile residual stresses in the substrate. 3-D stress/strain simulations reveal that the stress/strain distribution in the thin film is close to equi-biaxial. The current article will provide further experimental evidence that supports the findings in Part I through local characterization of the stress/strain fields in the shock treated metal thin film using X-ray microdiffraction [5,6] and instrumented nanoindentation [7].

2 Sample Preparation

All substrates used in the current study were 6″ diameter 0.5 mm thick single crystal silicon (SCS) wafers with the ⟨004⟩ direction nominally parallel to the surface normal. On some substrates, PVD copper thin films of 1 and 1.5 micron thicknesses were deposited at room temperature and 2 mTorr chamber pressure. On others, 3 micron thick Cu films were electrochemically plated. Before electroplating, a 25 nm TiN layer was deposited as a barrier layer, and a 15 nm copper seed layer was sputtered on the barrier layer. The deposited wafers were then sliced into 12 mm by 20 mm rectangular pieces (Fig. 1).

A Q-switched Nd:YAG laser with pulse duration of 50 ns and wavelength of 355 nm was used in the shock peening experiments. During laser shock peening, the sample was covered with an aluminum foil of 16 μm thickness, with a very thin layer of vacuum grease in between. Thermal effects were isolated from the sample and only shock effects are experienced by the sample [4]. The laser beam was about 12 microns in diameter. Three pulse energy levels, 244, 209, and 174 μJ, corresponding to laser intensities of 4.31, 3.67, and 3.08 GW/cm^2, respectively, were used. As seen from Fig. 1, the copper film of the sample is shock peened either along a line (Fig. 1(a)) or along seven parallel lines in the central region of the samples. The spacing between consecutive laser pulses along each line is 25 microns and the spacing between adjacent lines is also 25 microns. A sticky tape was applied on one side of the sample and laser scribing of the tape was used to mark the location of the shocked region for positioning purpose during material characterization because the shocked lines were not visible on the Cu films.

3 X-ray Microtopography and Microfluorescence Experiments

These experiments were conducted at the X20A beamline of the National Synchrotron Light Source at Brookhaven National Laboratory using the IBM microdiffractometer (Fig. 2). This instrument is a standard two-circle Huber diffractometer equipped with limited-range chi and phi stages for sample orientation, Oriel micrometer stages for precise and accurate sample positioning and a tapered capillary optic mounted on an Eulerian cradle for defining the incident beam. A vacuum chuck or adhesive film is used to hold the sample in place during the experiment. Placement of the region-of-interest in the x-ray beam is achieved visually through two CCD cameras equipped with telescopic lens. The incident beam is monochromatic, and the beam energy can be set by the user in the range of 6-10 keV. The irradiated area on the sample is in the form of an ellipse, the major diameter of which equals the minor diameter at normal incidence. The instrument is equipped with energy-dispersive (SiLi) and scintillation detectors for mapping sample fluorescence and diffraction signals respectively. Further details of the instrument and experiment methodology can be found in references [5,6] and [8,9].

In the current study, 9.1 keV X-rays were used to map Cu fluorescence as a function of sample position. The fluorescent
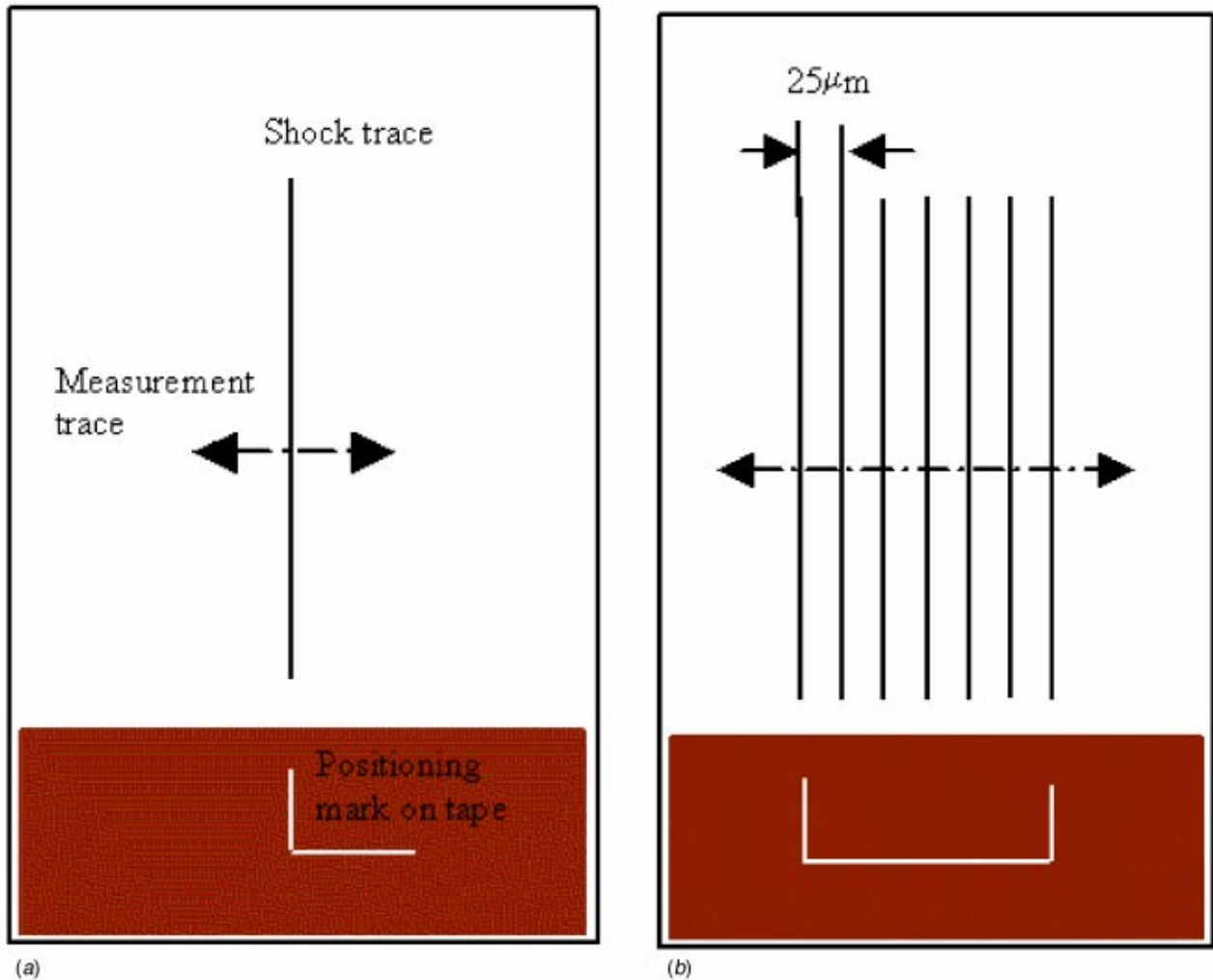
Fig. 1 Illustration of sample preparation; sample size: 12 by 20 mm; sample materials: copper thin film on single crystal silicon (004) substrate; the film is shocked along (a) a single line, or (b) 7 parallel lines, both at the central region of a sample; and sticky tapes are applied at an end of a sample with laser scribed marks to facilitate positioning in subsequent X-ray microfraction and nanoindentation measurements
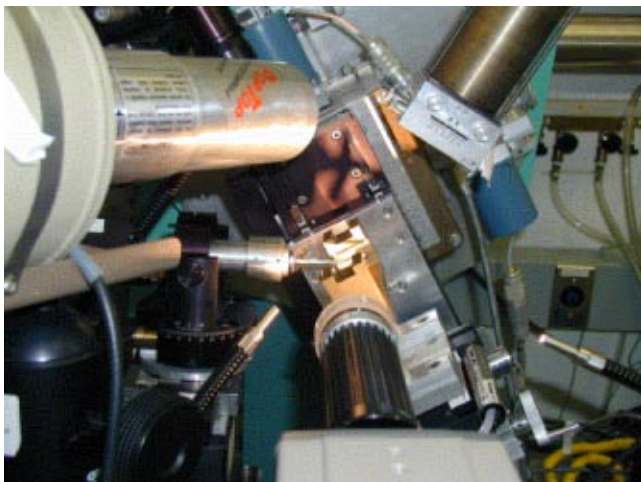

Fig. 2 Experimental setup of the X-ray Microdiffraction Experiment (Courtesy of Dr. S. Kaldor)

yield is linearly related to the volume of the irradiated material. Thus, when the film thickness is less than the penetration depth of X-ray, the variation of film fluorescence yield can be used to monitor the film thickness variations in the scanned areas. X-ray microtopography of the underlying Si substrate was carried out by mapping the integrated intensity of the Si 004 reflection at nominally 65° 2θ with 8.5 keV ($\lambda = 1.459$ Å) X-rays. The integrated intensity of single crystal reflections is proportional to the non-uniform strains in the diffracting volume [10–12], with higher intensities indicating regions of higher strain. In the current experiments, the position of the shocked region relative to the X-ray beam was carefully calibrated. Then, the Bragg angle of the Si 004 reflection was optimized at a location away from the shocked region by maximizing the integrated intensity using the appropriate sample tilts (θ and χ). Then, by scanning the sample relative to the beam in 4 or 2 microns step size, the distribution of the Si(004) diffraction intensity across the shocked region was recorded. Samples of three thicknesses treated at various conditions were tested.
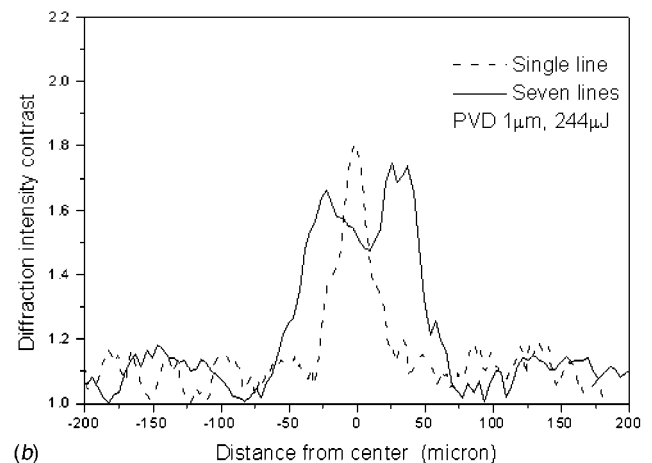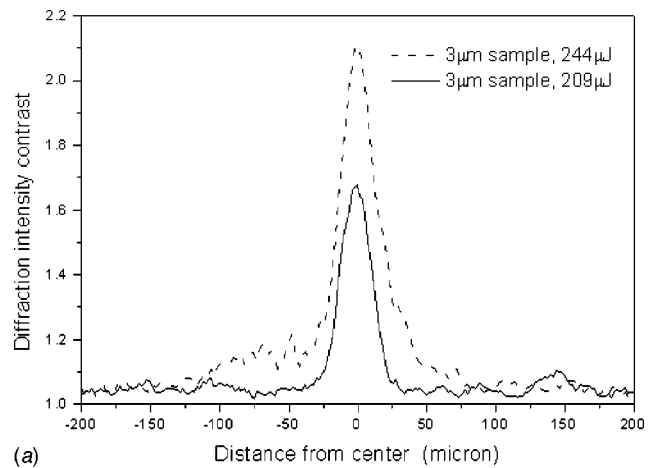
The spatial resolution of conventional X-ray diffraction is typically larger than 0.5 mm. It was used to measure the average stress/strain [4] but is too large to measure the stress/strain distributions in microscale laser shock processing. The X-ray microdif-
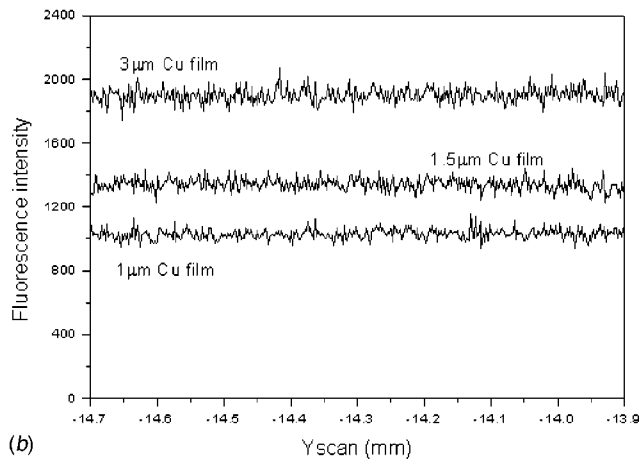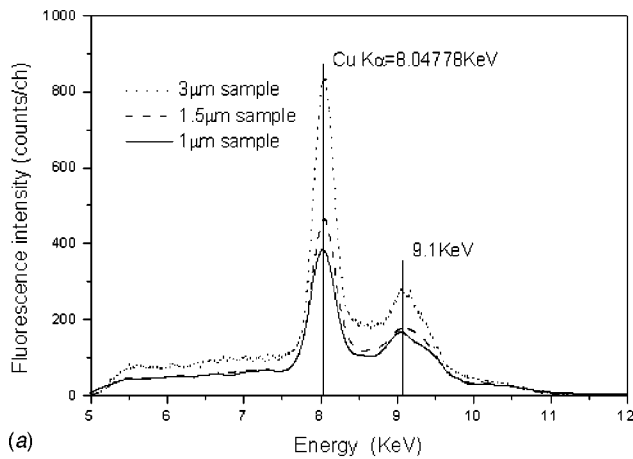
Fig. 3 Fluorescence measurement of un-shocked copper thin films with X-ray energy at 9.1 KeV (*a*) Fluorescence spectra of the copper thin films; and (*b*) Fluorescence intensity distribution across the film surface, step size 2 microns

Fig. 4 Si (004) diffraction intensity contrast across the shocked region measured in 2-micron step size. (*a*) pulse energy of 244 μJ and 209 μJ, 3 μm sample, single line shocking; and (*b*) Comparison of single line and 7 line shocking results, pulse energy of 244 μJ, 1 μm sample. The diffraction intensity is normalized to the average background diffraction intensity (14000 counts).

fraction experiments reported in this paper characterized the stress/strain fields with micron-level spatial resolutions. High brightness X-ray beams are needed for speed and accuracy in X-ray microdiffraction experiments. Otherwise, a long sampling time is required to yield meaningful results, and the accuracy can suffer from drifting and noise in slow and low intensity measurements. For this reason, synchrotron radiation sources were used. The high brightness X-ray beams from synchrotron radiation sources were narrowed down and then focused to micron spot size using a tapered glass capillary. The lead glass capillary is parabolic in shape, the incident bore diameter is about 50 μm, the exit bore diameter is about 5 μm, and the length is about 8cm (Fig. 2). It focuses the beam to a small spot size (about 10 microns on the sample surface) through total external reflection and increases the gain of the system (defined as the intensity at the exit of the capillary to the intensity at entrance) by tens of times [13]. Both small spot size and increased intensity are desired in X-ray microdiffraction.

3.1 Results and Discussions. The primary purpose of the fluorescence measurement in this study is to monitor the surface integrity of the films. Figure 3(*a*) shows the X-ray fluorescence spectra of copper films of different thicknesses. In all cases, the spectra consists of two peaks; one from the Cu $K\alpha_1$ fluorescence at 8.05 keV and the other from elastic scattering of the primary beam at 9.01 keV. As expected, the fluorescence intensity changes monotonously with film thickness. During X-ray scans the integrated intensity of the Cu fluorescence peak was recorded at 2

micron intervals along a line 800 micrometers in length on the sample surface. This data are shown in Fig. 3(*b*) for the three films. The intensity traces are all horizontal, with very small point-to-point variations indicating good thickness uniformity of the films.

The profiles of Si (004) diffraction intensity contrast across the shocked region by a line of shocks of the 1 μm sample has been shown in Part I of this paper and prominent peaks are observed in the shocked region. The intensity contrast profiles for 3 μm samples processed at 244 μJ and 209 μJ are shown in Fig. 4(*a*). A similar trend as in the 1 μm sample is observed. However, under the same energy levels, the intensity contrasts of the 3 μm sample are larger than those of the 1 μm sample. This indicates that a stronger local nonuniform strain field is induced in the Si under the thicker films under the same conditions. Since the Si stress field is balanced by stresses in the film, the stress state in the thicker films are also expected to be higher. The diffraction intensity contrast peak is due to shock effects, as further verified by the comparison of the results of single line and 7 lines for the 1 μm sample at 244 μJ (Fig. 4(*b*)). The profile of the 7 lines case shows a much wider peak than the single line case, covering a region about 150 microns, which is close to the total span of shock treated region (Fig. 1).

The peak values of diffraction intensity contrast under various
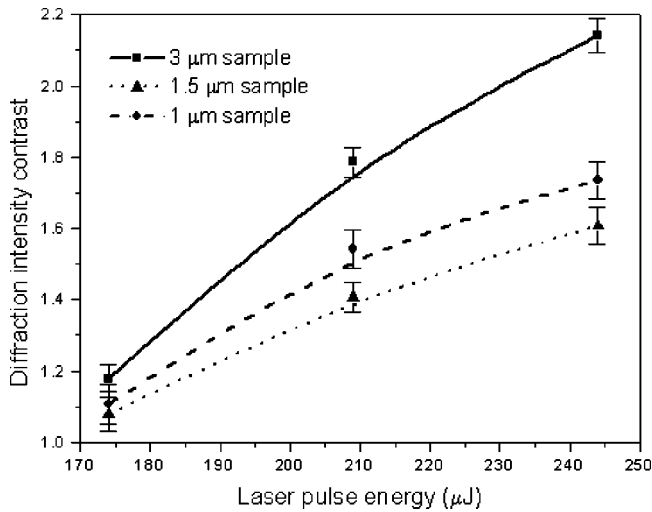
Fig. 5 Variation of diffraction intensity contrast with laser pulse energy and film thickness. Each data point represents the average of three measurements, standard error is used to plot the error bars, and smooth lines are fitted through these data points. The diffraction intensity is normalized to the background diffraction intensity counts

conditions are compared in Fig. 5. For the same film thickness, with the increase of pulse energy, the diffraction contrast increases, and a trend of leveling off at high laser pulse energy can be seen in all three curves. Under the same level of laser pulse energy, it is observed that the thicker the film, the higher the contrast of diffraction intensity. Thicker films have longer time to absorb the shock energy than thinner films, and under the same level of laser pulse energy, the stress/strain fields at the interface are stronger in thicker films than in thinner films, as shown by simulations (Fig. 6).

3.2 Strain Modeling and Comparison with X-ray Microdiffraction Results. The location of stress/strain concentration and relative change of stress/strain in metal thin film can be inferred from the diffraction contrast of the substrate [6,9]. It has also been shown that the diffracted intensity varies monotonically and non-linearly with the "bending strain" [10], but the quantitative correspondence between local stress/strain and the increase in diffraction intensity is a complex problem and is still under investigation [14]. In experiments, it is difficult to find a suitable and
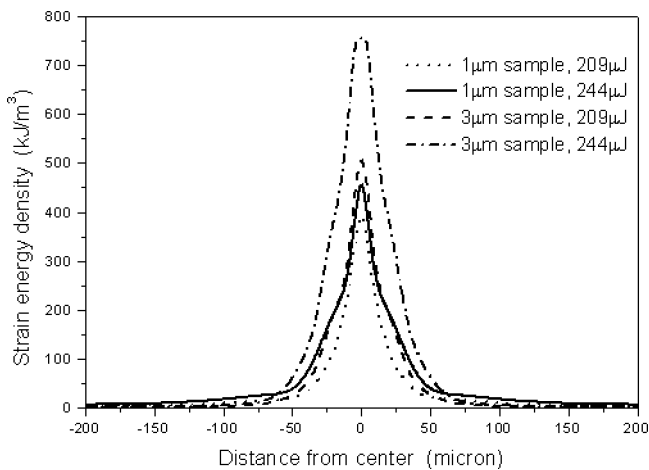
Fig. 6 Simulation results of the strain energy density at the copper-silicon interface

measurable index to represent the degree of imperfection of the lattice. Numerical simulations do not have the limitations of experiments, such as spatial resolution or extracting variables from the interior of the sample. Stress/strain numerical analysis of the thin film structure has been discussed in Part 1 of this paper. Comparison of the experimental results with the simulation results may shed light on the quantitative correlation between the stress/strain field and the X-ray diffraction intensity contrast.

In this study, various efforts were first made to correlate strain or stress components in simulations with the X-ray diffraction intensity contrast. But it turned out that the region of substantial elastic strain or residual stress in the film is much greater than that of the contrast peaks, while the region of substantial plastic strain is less than that of the contrast peaks. Going back to the origin of the X-ray diffraction intensity contrast, the increase of diffraction intensity comes from the increased band-pass in the substrate induced by the nonuniform stress/strain field in the thin film at the interface. An index evaluating this combined effect is perceived as strain energy density D which is defined as [15]:

$$D = \frac{1}{2}\varepsilon_{ij}\sigma_{ij} = \frac{1}{2}(\varepsilon_{11}\sigma_{11} + \varepsilon_{22}\sigma_{22} + \varepsilon_{33}\sigma_{33} + \varepsilon_{12}\sigma_{12} + \varepsilon_{13}\sigma_{13}$$
$$+ \varepsilon_{23}\sigma_{23}) \tag{1}$$

where ε_{ij} is the total strain (elastic plus plastic) tensor and σ_{ij} the residual stress tensor. The unit of D is J/m^3.

Strain energy density is difficult to measure experimentally, but its value can be readily extracted from simulation. Single crystal silicon is strongly anisotropic. The estimation of strain energy density in silicon may not be highly accurate due to the isotropic assumption in simulation. The copper thin films used in this study are close to isotropic, which agrees with the assumption in simulation. Thus, effort is focused on relating the simulated strain energy density of copper to the experimental results of X-ray diffraction intensity contrast. This is a reasonable assumption, given that the two stress fields are related through the force balance. Figure 7 compares the strain energy densities in copper at the interface under the same conditions as those for the X-ray diffraction experiments. First of all, simulation results indicate that the strain energy density is higher for higher pulse energies and greater film thicknesses. Similar trends are observed for the diffraction contrast levels as in Fig. 4 and Fig. 5.

Profiles of X-ray diffraction intensity contrast of single line shock processed 1 μm and 3 μm samples are compared with the profiles of strain energy density in Fig. 7(*a*) and (*b*), respectively. The fluctuations outside the peaks are within experimental error while the central peaks undoubtedly agree with the shock treated region. The profiles from simulation and from X-ray experiment come into good agreement when the magnitude of strain energy density is shifted and divided by a suitable value (see Eq. (2)). Both 1 μm and 3 μm samples show a single central peak. For the 7-lines case of the 1 μm sample, however, both the intensity contrast in the X-ray experiment and the strain energy density in simulation show a saddle shaped peak (Fig. 7(*c*)). The simulation result predicts a slightly wider distribution of the saddle shaped peak than X-ray experiments, but the difference is within the range of experimental error. Stress/strain is relatively uniform within the shocked region in the case of 7-lines, but the transition from a uniformly shocked region to a shock free region results in stress concentration. Strain energy density increases in these transitional regions, which is the cause of the saddle shape in Fig. 7(*c*).

The fact that both peak location and shape show a good agreement indicates that the two quantities may be linearly related. Let XDC be the X-ray diffraction intensity contrast, and D the strain energy density as defined in Eq. (1), an empirical relation is inferred from Fig. 7
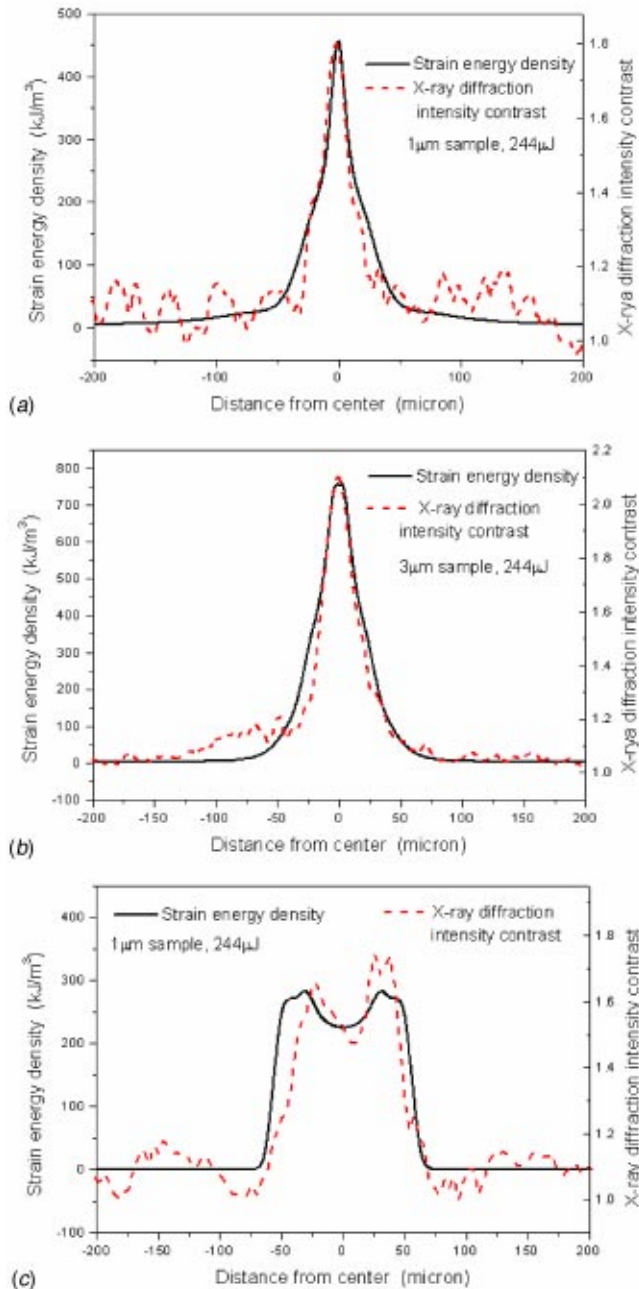
Fig. 7 Comparison of strain energy density (solid line) and X-ray diffraction intensity contrast (dashed line) (a) 1 μm sample, 244 μJ, single line; (b) 3 μm sample, 244 μJ, single line; and (c) 1 μm sample, 244 μJ, 7 lines

$$D \approx K(XDC-1) = \frac{\max(D)}{\max(XDC-1)}(XDC-1) \qquad (2)$$

Under the condition of equi-biaxial stress distribution, Eq. (2) reduces to:

$$\varepsilon_{11}\sigma_{11} = \varepsilon_{22}\sigma_{22} \approx K(XDC-1) \qquad (3)$$

where K is a proportional coefficient. This linear correlation is relatively well obeyed under other conditions in this study. Current experiments show that the value of K is case dependent, but for each case a value of K can be found to draw the experimental and simulation profiles closer to match. The determination and the physical meaning of coefficient K require further experimental

and theoretical investigation. For equi-biaxial stress distribution, the linear correlation between strain energy density and X-ray microdiffraction contrast makes it possible to decide the strain field gradient directly from the measurement of X-ray diffraction intensity contrast since stress and strain are correlated by material constitutive equations. Be noted that this empirical correlation may not hold under other conditions or other materials and more detailed studies are required.

## 4 Characterization of the Shocked Sample Using Instrumented Nanoindentation

Laser shock peening can induce plastic deformations in the copper thin film, thus should increase its hardness. Improved hardness is beneficial for metal MEMS structures with rubbing surfaces. But hardness improvement for thin metal films treated by laser shock peening has not been seen in the literature. The micron-level in the film thickness and in the shock-affected region requires that high spatial resolution method be used in the measurement of thin film hardness. Instrumented nanoindentation is used for this reason.

Instrumented nanoindentation provides a continuous record of the variation of indentation load, P, as a function of the depth of penetration, h, into the indented specimen. Comprehensive theoretical and numerical studies have been carried out to elucidate the contact mechanics and deformation mechanism in order to systematically extract material properties from the P versus h curves [16–18]. The P-h curves have been used to obtain many material properties, such as hardness, Young's modulus, yield strength, and work hardening exponent [19–21]. Of special interest is that instrumented nanoindentation can be used to estimate the sign and magnitude of the stress/strain field in thin films [7]. Before extracting hardness and the sign of stress/strain field from instrumented nanoindentation, the assumptions and limitations are first discussed.

The numerical simulations [17,18] assume that the indentation is a frictionless, quasi-static indentation of an isotropic elastoplastic substrate by an elastic indenter, and the indented substrate is permitted to undergo isotropic strain hardening. This assumption is reasonable for nanoindentation of ductile metals using diamond Berckovich indenters [18]. The analysis is valid within the continuum mechanics regime, that is, the indented area should cover at least five grains of the substrate material. It is also assumed that the residual stress in the sample is or is close to equibiaxial, i.e., $\sigma_{11} = \sigma_{22}$, and the stress should be uniform within a depth of at least 3 times the width of the indenter contact radius [20].

A line of shocks (Fig. 1(a)) is applied to each of the samples used in the nanoindentation tests. After sufficient stress relaxation, the thin film is in plane-stress state, and the stress/strain is nearly uniform throughout the depth of the film. Numerical simulations in Part I of this paper reveal that the in-plane stress/strain components vary in magnitude gradually from a high value at the shocked center to zero at a distance about 75 microns from the center. Strictly speaking, this is not equi-biaxial stress distribution. However, the equi-biaxial assumption can be considered to apply locally because the nanoindentation test used in this study each time measures only a small region (the dent diameter is less than 1 micron) of the thin film, and within the measured volume the stress/strain can be considered uniform.

If there are pre-existing residual stress and/or pre-existing plastic strains, the indentation of the specimen will be influenced by the stress/strain field. The equi-biaxial tensile stress in a film is equivalent to the combination of a hydrostatic tensile stress plus a differential compressive stress in the in-depth direction. This differential compressive stress is in the same direction as indentation. Thus, tensile residual stress aids indentation by increasing the contact area for a given indentation load or by lowering the indentation load needed to penetrate the material to a certain depth. On the other hand, the equi-biaxial compressive residual stress in
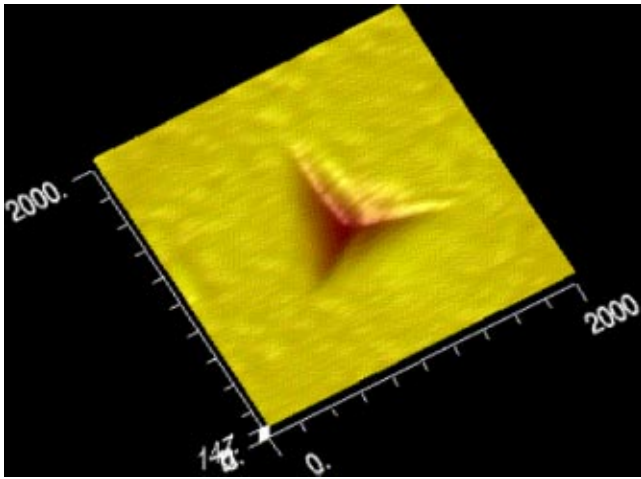
Fig. 8   3D image of the indention on the un-shock 1 μm copper thin film on silicon substrate. Berkovich diamond nanoindenter leaves a triangular dent in the sample. The unit in the image is nm. The full scale in the depth direction is 147 nm. The maximum loading is 1000 μN.

Fig. 9   Hardness distribution across shocked 1 μm samples measured using nanoindentation

the film is equivalent to the combination of a hydrostatic compressive stress plus an in-depth direction tensile stress. This differential tensile stress is in opposite direction of the indentation and tends to impede indentation. Thus, the method of instrumented nanoindentation can be used to decide the sign and estimate the magnitude of the stress/strain field in shock treated thin films in addition to hardness [20].

4.1   Experiments.   Shock treated 1 μm samples are tested using a Triboscope Nanomechanical Test System from Hysitron Inc. The loading/unloading curves are recorded digitally. The system calculates the value of hardness P_{ave} (=maximum load/true contact area) directly, with the noises in measurement accounted for. Based on repeated measurements reported by Suresh and Giannakopoulos [20], the Young's modulus of the copper thin film in this study uses a fixed value, $E_f = 126$ GPa. The Poisson ratio is $\nu_f = 0.38$, taken from bulk material. The Young's modulus and Poisson ratio of the diamond Berkovich nanoindenter used are: $E_i = 1140$ GPa and $\nu_i = 0.0707$. The included angle of the Berkovich indenter tip is 24.7°. The effective Young's modulus of the indenter-specimen system is defined as [7]:

$$E^* = 1/\left(\frac{1-\nu_f^2}{E_f} + \frac{1-\nu_i^2}{E_i} \right) \tag{4}$$

Thus, $E^* = 130.49$ GPa. In all of the measurements the maximum load is fixed at 1000 μN, and the loading and unloading rates are both 100 μN/s. The shocked region is scanned perpendicular to the centerline (Fig. 1(a)), with the spacing between consecutive indenting points of 12.7 microns.

4.2   Results and Discussion.   Figure 8 shows the 3D image of the indention on the shock-free 1 μm copper thin film sample using a maximum loading of 1000 μN. From the image, it is seen that the contact radius of the indenter is about 0.4 microns. The grain size of the thin film is 0.1-0.2 microns. Thus the assumption of continuum mechanics is basically satisfied. The dent depth is controlled to be less than one-eighth of the film thickness in order to reduce the influence of the substrate.

Compared with the shock free region and despite the scattering in the data, the trend of increase in hardness in the shock treated region is unmistakably seen in Fig. 9. The maximum hardness is increased by more than 11% under both pulse energy of 244 μJ and 209 μJ. The hardness at 244 μJ is only slightly larger than the hardness at 209 μJ. The increase of hardness arises from two
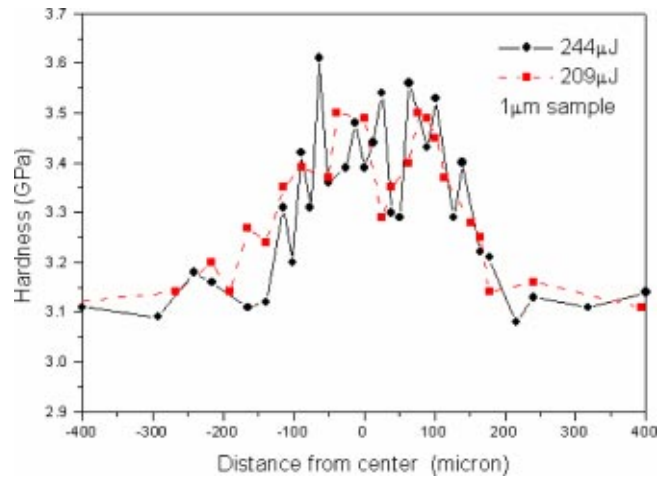
causes: one is work hardening due to plastic deformation (in a narrow central region only) and the other is the compressive residual stress in the shock treated region.

The hardness of annealed bulk copper measured by conventional hardness testers is 400 MPa, and the hardness of cold hardened bulk copper is 1 GPa [22]. Neither the nano- nor microhardness is a fixed value. Both vary with the applied load. For example, the nano-hardness and the micro-hardness of the same bulk copper sample obtained by consolidating nanocrystalline powders were measured to be 2.42 GPa and 1.88 GPa, respectively [23]. Antunes et al. [24] reported the micro-hardness of bulk copper measured by a Vickers indenter to be 1.7 GPa. The hardness of bulk copper is not directly comparable with the thin film hardness. Due to much reduced thickness, the strength and hardness of the thin film should be higher than those of the bulk material [25]. The hardness reported here is within a reasonable range. Hardness tests of PVD copper thin films are rare in the literature. As a comparison, Narayan et al. [26] reported that the nano-hardness of copper thin film on silicon (001) substrate prepared by pulsed laser deposition of nanocrystalline material varied in the range from 2 GPa to 12 GPa.

The sign of the stress, which cannot be decided using the X-ray microdiffraction method described in Section 3, can be decided by studying the loading/unloading curves in instrumented nanoindentation. The loading and unloading curves at different locations of the shock treated region are shown in Figs. 10(a) and (b), for pulse energy of 244 μJ and 209 μJ, respectively. From these curves, the signs of the residual stresses can be judged. The reference curve (the dashed line) was taken from regions far away (250 microns) from the shocked region. Compared with the reference curve, the loading curves close to the center of the shocked region shift leftwards, indicating that to reach the same penetration depth, a larger load is needed. This is indicative of compressive residual stress in the shock treated region as predicted by simulations.

Nanoindentation is a destructive testing method, and it is also very sensitive to environmental disturbances and local surface quality variations of the sample, such as defects and grain boundaries. All these factors lead to relatively large scattering in the testing data. Despite the scattering in the experimental data, the increase in hardness and the presence of local compressive residual stress in the shocked region are unmistaken, and the general trends in nanoindentation tests agree with the trends in curvature measurement, simulation and X-ray microdiffraction.
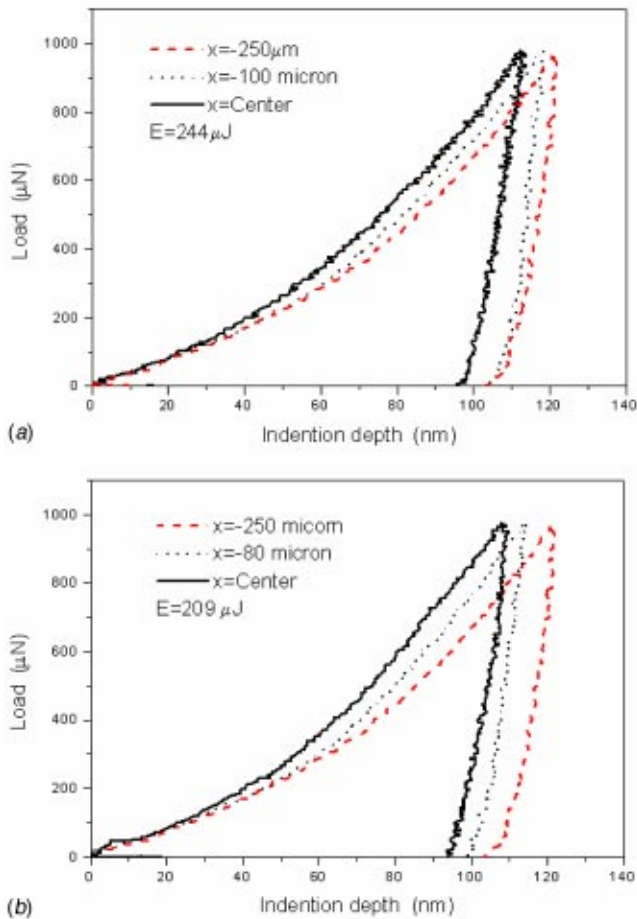
Fig. 10 Loading and unloading curves measured at different locations of shocked 1 μm samples (*a*) 244 μJ and (*b*) 209 μJ. The dashed line, measured far away (250 microns) from the shock center, represents the reference curve.

5 Conclusions

Microscale laser shock peening effects on copper thin films were experimentally measured and compared with numerical results. Laser shock processed copper thin films were characterized with micron-level spatial resolution using X-ray microdiffraction and instrumented nanoindentation. X-ray microdiffraction measurements based on intensity contrast method sensitively detected the region of stress/strain concentration with micron-level spatial resolution. It was found that X-ray diffraction intensity contrast might be linearly related to the strain energy density at the film-substrate interface under the conditions used in this study, while the physical meaning and the determination of this linear correlation requires further experimental and theoretical investigation. Nano-hardness in the shocked region increased by more than 11%, which is beneficial for the improvement of wear resistance of the metal film. Instrumented nanoindentation showed that the residual stress in the shock treated region was compressive.

References

[1] Miller, S. L., Rodgers, M. S., LaVigine, G., Sniegowski, J. J., Clews, P., Tanner, D. M., and Peterson, K. A., 1998, "Failure Modes in Surface Micromachined Micro-Electro-Mechanical Actuators," *IEEE 98CH36173, 36th Annual International Reliability Physics Symposium*, pp. 17–25.
[2] Tanner, D. M., Walraven, J. A., Helgesen, K. S., Irwin, L. W., Gregory, D. L., Stake, J. R., and Smith, N. F., 2000, "MEMS Reliability in a Vibration Environment," *IEEE 00CH37059, 38th Annual International Reliability Physics Symposium*, pp. 139–145.
[3] Zhang, W., and Yao, Y. L., 2000, "Improvement of Laser Induced Residual Stress Distributions via Shock Waves," *Proc. ICALEO'00, Laser Materials Processing*, Vol. 89, pp. E183–192.
[4] Zhang, W., and Yao, Y. L., 2002, "Micro Scale Laser Shock Processing of Metallic Components," ASME J. Manuf. Sci. Eng., **124**(2), pp. 369–378.
[5] Noyan, I. C., Jordan-sweet, J. L., Liniger, E. G., and Kaldor, S. K., 1998, "Characterization of Substrate/Thin-film Interfaces with X-ray Microdiffraction," Appl. Phys. Lett., **72**(25), pp. 3338–3340.
[6] Wang, P.-C., Noyan, I. C., Kaldor, S. K., Jordan-sweet, J. L., Liniger, E. G., and Hu, C.-K., 2000, "Topographic Measurement of Electromigration-induced Stress Gradients in Aluminum Conductor Lines," Appl. Phys. Lett., **76**(25), pp. 3726–3728.
[7] Suresh, S., and Giannakopoulos, A. E., 1998, "A New Method for Estimating Residual Stresses by Instrumented Sharp Indentation," Acta Mater., **46**, pp. 5755–5767.
[8] Noyan, I. C., Wang, P.-C., Kaldor, S. K., Jordan-Sweet, J. L., and Liniger, E. G., 2000, "Divergence Effects in Monochromatic X-ray Microdiffraction Using Tapered Capillary Optics," Rev. Sci. Instrum., **71**(25), pp. 1991–2000.
[9] Noyan, I. C., Wang, P.-C., Kaldor, S. K., and Jordan-Sweet, J. L., 1999, "Deformation Field in Single-crystal Semiconductor Substrates Caused by Metallization Features," Appl. Phys. Lett., **74**(16), pp. 2352–2354.
[10] Cullity, B. D., 1978, *Elements of X-ray Diffraction*, London, Addison-Wesley Publishing Company, Inc., Second edition, pp. 103, and pp. 268–270.
[11] Blech, I. A., and Meieran, E. S., 1967, "Enhanced X-ray Diffraction from Substrate Crystals Containing Discontinuous Surface Films," J. Appl. Phys., **38**, pp. 2913–2919.
[12] Segmüller, A., Angilelo, J., and La Placa, S. J., 1980, "Automatic X-ray Diffraction Measurement of the Lattice Curvature of Substrate Wafers for the Determination of Linear Strain Patterns," J. Appl. Phys., **51**(12), pp. 6224–6230.
[13] Erko, A. I., Aristov, V. V., and Vidal, B., 1996, *Diffraction X-ray Optics*, Philadelphia, Institute of Physics Publishing Ltd, pp. 2–15.
[14] Gilvarry, J., Chowdhury, A. K., Monclus, M., Cameron, D. C., McNally, P. J., and Tuomi, T., 1998, "Stress Behavior of Reactively Sputtered Nitrogenated Carbon Films," Surf. Coat. Technol., **98**, pp. 985–990.
[15] Ventsel, E., and Krauthammer, T., 2001, *Thin Plates and Shells: Theory, Analysis and Applications*, New York, Marcel Dekker, Inc., pp. 37.
[16] Laursen, T. A., and Simo, J. C., 1992, "A Study of the Mechanics of Microindentation Using Finite Elements," J. Mater. Res., **7**, pp. 618–626.
[17] Giannakopoulos, A. E., Larsson, P. L., and Vestergaard, R., 1994, "Analysis of a Vickers Indentation," Int. J. Solids Struct., **31**, pp. 2679–2708.
[18] Larsson, P. L., Giannakopoulos, A. E., Soderlund, E., Rowcliffe, D. J., and Vestergaard, R., 1996, "Analysis of Berkovich Indentation," Int. J. Solids Struct., **33**(2), pp. 221–248.
[19] King, R. B., 1987, "Elastic Analysis of Some Punch Problems for a Layered Medium," Int. J. Solids Struct., **23**(12), pp. 1657–1664.
[20] Giannakopoulos, A. E., and Suresh, S., 1999, "Determination of Elastoplastic Properties by Instrumented Sharp Indentation," Scr. Mater., **40**(10), pp. 1191–1198.
[21] Dao, M., Chollacoop, N., Vliet, K. J. V., Venkatesh, T. A., and Suresh, S., 2001, "Computational Modeling of the Forward and Reverse Problems in Instrumented Sharp Indentation," Acta Mater., **49**, pp. 3899–3918.
[22] Grogoriev, I. S., and Meilikhov, E. Z., 1997, *Handbook of Physical Quantities*, New York, CRC Press, pp. 49.
[23] Srivatsan, T. S., Ravi, B. G., Naruka, A. S., Riester, L., Yoo, S., and Sudarshan, T. S., 2000, "A Study of Microstructure and Hardness of Bulk Copper Sample Obtained by Consolidating Nanocrystalline Powders Using Plasma Pressure Compaction," Materials Science and Engineering A, **311**, pp. 22–27.
[24] Antunes, J. M., Cavaleiro, A., Menezes, L. F., Simoes, M. I., and Fernandes, J. V., 2002, "Ultramicrohardness Testing Procedure with Vickers Indenter," Surf. Coat. Technol., **149**, pp. 27–35.
[25] Hutchinson, J. W., 2000, "Plasticity at the Micron Scale," Int. J. Solids Struct., **37**, pp. 225–238.
[26] Narayan, J., Sharma, A. K., Kvit, A., Kumar, D., and Muth, J. F., 2000, "Novel Nanocrystalline Materials by Pulsed Laser Deposition," Mat. Res. Soc. Symp., **617**, pp. J.2.4.1–6.